**Rapid Electrostatic Capture of Rod-Shaped Particles on Planar Surfaces: Standing up to Shear**

Molly K. Shave,[1] Aiste Balciunaite,[1] Zhou, Xu,[2] and Maria M. Santore[1,*]

[1]Department of Polymer Science and Engineering
University of Massachusetts at Amherst
120 Governors Drive
Amherst, MA 01003

[2]Department of Physics
University of Massachusetts at Amherst
666 North Pleasant Street
Amherst, MA 01003

Santore@mail.pse.umass.edu
413-577-1417

**Abstract**
We compare the electrostatically-driven capture of flowing rod-shaped and spherical silica particles from dilute solutions onto a flow chamber wall that carries the opposite electrostatic charge from the particles. Particle accumulation and orientation are measured in time at a fixed region on the wall of a shear flow chamber. Rod-shaped particle aspect ratios are 2.5 - 3.2 and particle lengths are 1.3 and 2.67μm for two samples, while sphere diameters were 0.72, 0.96 and 2.0 μm for three samples. At a moderate wall shear rate of 22 $s^{-1}$, particle accumulation for both rods and spheres is well described by diffusion-limited kinetics, demonstrating the limiting effect of particle diffusion in the near-wall boundary layer for electrostatically-driven capture in this particle shape and size range. The significance of this finding is demonstrated in a calculation that shows that for delivery applications, nearly the same (within 10%) particle volume or mass is delivered to a surface at the diffusion-limited rate by rods and spheres. Therefore, in the absence of other motivating factors, the expense of developing rod-shaped microscale delivery packages to enhance capture from flow in the diffusion-limited simple shear regime is unwarranted. Also interesting, the captured orientations of the larger rods, 2.6 μm in average length, were highly varied and insensitive to flow: a substantial fraction of rods were trapped in standing and slightly leaning orientations, touching the surface by their ends. Additionally, for particles that were substantially tipped over there was only modest orientation in the flow direction. Taken together these findings suggest that on the timescale of near-surface particle rotations, adhesion events are fast, trapping particles in orientations that do not necessarily maximize their favored adhesive contact or reduce hydrodynamic drag.

**Keywords:** rodlike, fiber, capsular, colloid, deposition, rod particle adhesion, rod particle deposition

## Introduction

The capture of flowing microparticles on the surfaces of channels and porous media is critical in a variety of situations and technologies: membrane filtration, the delivery of drugs to the vasculature, the transport of bacteria in ground water, microfluidics, complex fluid handling, and in biomedical devices such as catheters and intravenous lines where bacteria may be retained. By comparison to the large body of work focusing on spherical particles,[1-6] precise experimental studies of non spherical particles, even those with symmetric shapes such as disks and rods, are limited. Thus the question remains: when can the transport and capture of non-spherical particles be approximated by that of equivalent spheres and how does shape influence the configuration of particles retained on surfaces?

In complex fluids such as blood, disks, rods, and spheres reach a flow channel wall with different efficiencies as a result of specific mechanisms, for instance multibody effects such as margination,[7, 8] or those resulting from the curvature of streamlines.[9, 10] However, even in the basic case of a dilute suspension in simple shear, expectations for the transport and adhesion of rods (and disks) are not well-developed and lack consensus on experimental confirmation. Theoretical works often isolate a single mechanism (in the case of transport for instance: diffusion, viscous effects,[11] and inertia.[12, 13]) However, multiple mechanisms likely come into play in experiments that target the conditions in applications.

Relevant to microparticle rods in the dilute limit, models for rod diffusion in a quiescent liquid[14, 15] were critically refined as recently as 2003,[16] and experimental methods for tracking rotational rod diffusion were developed in 2007.[17] Shear flow introduces a torque that, in the absence of

diffusion, produces closed rotational trajectories[11, 18] or, in the presence of diffusion, can alter diffusivity by altering the rod orientation.[19, 20] The impact of a boundary on a rod subject to viscous shearing forces has been addressed relatively recently.[21, 22] With diffusion suppressed so that viscous effects dominate, flagella-free *E. coli* (which are non-motile short rod shaped particles) follow a modified Jeffrey orbit and travel along a surface with their center of mass at a fixed distance from the surface.[23] Therefore compared with spheres, one might expect that the micron-scale separation of a rod particle from the surface in the moments when it is oriented parallel to the surface would reduce the capture efficiency of the particle on an otherwise adhesive wall. Separately, even for spheres, rotation of near wall particles has been shown to limit particle capture when discrete adhesive functionality (chemical heterogeneity[24] or ligands[25]) must engage to facilitate capture. One would therefore expect that at some conditions, at least, rotating or rolling of a near-surface rod will profoundly influence the probability of capture and arrest.

Some experiments inspired by delivery applications compare rod and spherical microparticles of identical volumes, with rod samples formed by stretching the spherical particles.[26, 27] In one such study, 1 μm spheres were found to adhere slightly more efficiently than rods (with aspect ratio near 8) but for larger spheres and equivalent rods, rod capture was preferred by a factor of 3-4.[26] A study with smaller sphere and rod particles, with the rods also produced by the stretching method, revealed much greater capture of spheres (up to six fold depending on ionic strength in a flow QCM) compared with equivalent rods.[27] Separately, lithographically produced porous silicon disks were captured from flow on the channel floor with substantially greater efficiency than similar flat-sided rods.[28] The critical difference in these systems, beyond particle size and

the impact of gravity, may be surface chemistry (influenced by the stretching process[27]) and the binding kinetics of surface moieties. Modeling efforts to predict the relative delivery efficiencies of particles of different shapes have included hydrodynamic forces on adhered particles (relevant to retention or pull off) [28, 29] but not particle flow or capture itself. Thus these treatments cannot be considered truly predictive of the delivery process. Treatments addressing the capture of non-spherical particles from flow are extremely recent, for instance finding that rods adhere with greater efficiencies from flow than spheres, due to their near-wall tumbling.[30] Other simulations do not cover a sufficient range of conditions to guide or compare with experiments.[9]

In summary, the current state of understanding for the adhesive capture of rods from flow is contradictory, with some groups reporting that rod capture is more efficient and others arguing lower efficiency relative to sphere or disks in shear flow. The discrepancy occurs across a particle size range, from 0.5 to 3 μm, but may be a result of the impact of gravity, surface chemistry (including ligand-receptor choice), particle polydispersity, and detailed particle shape. For instance differences between true rods, rice-shaped ellipsoids, and flat-sided "rod" cutouts can critically influence particle-wall contact during particle capture.

As illustrated in the schematic of Figure 1, this paper presents an experimental comparison of adhesive capture rates of flowing monodisperse rods (aspect ratios in two samples are 2.5 and 3.2) and spheres. Capture is facilitated by strong electrostatic interactions: the attraction of the negative silica particle surfaces to a channel wall functionalized with a polycationic coating. The wall shear rate near 20 $s^{-1}$ falls in the moderate range, relevant to fluid flow in the body, microfluidics, droplet drying, and bacterial capture during infection, as examples.[31-33] Also, the

flow chamber is oriented so that gravity does not drive particles towards or away from the surface. The study is significant in its quantification of the expected particle deposition rate in case transport limited capture as a benchmark. This requires knowledge of the bulk solution particle concentrations and dilute solution diffusion coefficients. We report, for the larger rod specimen, the extent to which captured rods are oriented on the channel wall. The results are put in the context of other studies of rod capture from the literature in terms of the kinetics of the capture binding events.

This work focuses on the dilute solution regime with volume fractions as high as 0.05% and where there is no impact of particle concentration for volume fractions at least 5 times this value. The particle Peclet numbers in this study fall in the range 1-10, for particles in the crucial near wall region, suggesting that particle convection and hydrodynamic-driven rotation compete with diffusion, while inertial effects are not important. (The relative inertial and viscous effects are described by the Stokes number,[13] with $St < 10^{-8}$ in this work, so inertial drift does not occur).

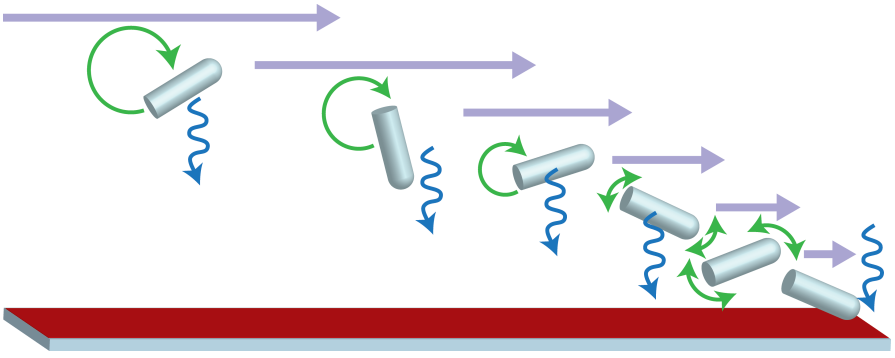

**Figure 1**. Shear flow drives particle translation and rotation away from the wall, dominating diffusion. Near the surface, shear is weaker so that both rotational and translational diffusion may be important or rate liming for particle-wall interactions, a prospect considered here. Also in this system, electrostatic attractions between cationic functionality on the wall and negative surface charge on the rods may drive rapid and strong particle capture once particles are within range of the wall. While the schematic of Figure 1 is oriented for ease of viewing, the flow chamber is oriented with the surface perpendicular to the floor and flow parallel to the floor.

**Experimental Methods and Procedures.**

***Rod-shaped silica particles***

Rod-shaped silica microparticles were synthesized following the one-pot method of Kuijk *et al*.,[34-36] established to produce samples with controlled particle sizes and aspect ratios in the micron and slightly submicron size range. Briefly, 25 mL ethanol, 6.7 mL ammonia (25% in water, EMD Millipore), and 7 mL deionized (DI) water were added to a polyvinylpyrollidone solution (PVP) comprising 25 g PVP ($M_n$= 40,000 g/mol, Sigma Aldrich) in 250 mL 1-pentanol (Sigma Aldrich). 1.1 mL sodium citrate dehydrate (0.18 M Sigma Aldrich) was then added to produce an emulsion, followed by the addition of 2.5 or 3.0 mL of tetraethylorthosilicate (TEOS, Sigma Aldrich) to grow the smaller or larger particles, respectively. The synthesis of the large rods included an addition of 3.0 mL TEOS, each after 6 hours.

After the synthesis of these "core rod particles," the particles were washed by centrifugation at 1500 g for 1 hour and resuspended in ethanol by vortexing and sonication. Samples were then washed by centrifugation (1500 g, 15 minutes) 2 more times with resuspension in ethanol, followed by 3 washes and resuspension in DI water. Up to 13 additional washes with resuspension in DI water were conducted at lower centrifugation speeds (eg 700 g) to reduce polydispersity and remove fines.

With the core rods satisfactorily monodisperse, as confirmed by SEM, a layer of Stöber silica[37] was then grown on their surfaces, to ensure uniform surface chemistry and to eliminate porosity and surface inhomogeneity caused by the presence of any residual PVP. Core rods were dispersed in 125 or 200 mL ethanol (for the small and large particles, respectively.) Ammonia

solution (15 mL for the small particles, 24 mL for the large particles) and DI water (12.5 mL for the small particles and 20 mL for the large particles) were added while stirring with a magnetic stirrer. TEOS was then added (0.25 and 1.0 mL for the small and large particles respectively) with continued stirring for at least 2 hours. Particles were then purified and fines removed with the same centrifugal washing procedures described for the core rods. Up to 40 additional washes were executed to ensure a lack of fines.

***Spherical silica particles.***

Two batches of silica microspheres (965 nm and 720 nm diameters) were synthesized following the Stöber method.[37] Ethanol (147.6 mL) , DI water (18.4 mL), and 25% ammonia solution (22.8 mL) were mixed. To this, TEOS (11.2 mL) was added while stirring. Stirring with a magnetic stirrer continued for 6 hours. One additional TEOS aliquot (and a stoichiometric amount of water) was introduced for the 720 nm particles and 4 additional TEOS aliquots were added over time (with a minimum time between aliquots of 6 hours) to produce the 960 nm particles. Particles were washed by centrifugation at 700 g for 15 minutes and resuspended 3 times in ethanol. They were additionally centrifuged and resuspended 3 times in DI water followed by 3 times in dilute phosphate buffer (5.9 mM, pH 7.4, 0.00182M $Na_2HPO_4$ and 0.000456 M $KH_2PO_4$.)

Additional studies employed 2 μm-diameter silica spheres purchased from Bangs Labs.

***Particle Characterization***

At critical stages in synthesis and purification particles were characterized by scanning electron microscopy (SEM) using a FEI Magellan 400 XHR instrument and by dynamic light scattering (DLS) and electrophoretic mobility (zeta potential) using a Malvern Zetasizer Nano. The Zetasizer was able to measure the zeta potentials of -73± 4 mV and -64± 3 mV for the 720 nm and 960 nm silica spheres, respectively. The 2000 nm particles from Bangs Labs and the rod samples appeared to possess the expected negative charge, however, the data from the Zetasizer were not convergent and not reportable, perhaps due to particle settling on the experimental timescale. For these reasons the electron micrograph data were determined to be more reliable for large rod particles than DLS measurements.

***Particle Capture from Flow and Orientation***

Particle capture was studied in a laminar slit flow chamber whose dimensions were large relative to those of the particles: 700 μm deep by 5.9 mm wide and 4.5 cm long. A functionalized glass microscope slide or coverslip comprised the chamber wall onto which particle capture was studied. Slides and coverslips were soaked overnight in concentrated sulfuric acid, rinsed with DI water, air-dried, and immediately sealed in the flow chamber. The chamber was then filled with flowing pH 7.4 phosphate buffer (0.008 M $Na_2HPO_4$ and 0.002 M $KH_2PO_4$), followed by flowing a 100 ppm solution of poly-l-lysine hydrobromide (PLL, nominal molecular weight 15,000-30,000 g/mol, Sigma) in phosphate buffer for 10 min, sufficient to saturate the surface. Then flowing phosphate buffer was reinjected to remove free polymer chains. This procedure for the deposition of a PLL layer was conducted at a wall shear rate of 5 $s^{-1}$ and functionalized

the channel wall with cationic charge. Previous studies established the complete retention of the PLL layer over a large range of conditions including the particle capture studied here.[4]

Particle capture was studied by flowing suspensions of particles through the flow chamber, which was mounted in a custom lateral microscope. Particle capture studies commenced immediately after the PLL layer was rinsed free of excess PLL, as described. The functionalized microscope slide or coverslip was oriented perpendicular to the floor and optical components were positioned on an optical bench. This arrangement avoided the influence of gravity on particle interactions with the surface. Particle suspensions were flowed through the chamber for ~10 minutes at a wall shear rate of 22 $s^{-1}$ employing a syringe pump, and their accumulation monitored at fixed region on the chamber wall. In the majorities of studies, particle flow and capture was monitored using a 20x phase contrast objective producing a viewing field of 260 μm x 177μm. For the larger rod particle sample, however, a 10x phase contrast objective was employed to view a larger area of surface, 480 μm x 340 μm. This was necessary because with a larger mass per particle and slower particle diffusion, the number of particles on the surface was substantially smaller (necessitating a larger field to obtain statistically significance). Additionally, in studies of captured rod orientation, a 40x objective was employed. Video data were exported to stacks of TIFF files using FFmpeg software. These image stacks were analyzed using manual tracking in *FIJI is just ImageJ*. Orientation was determined by measuring the angles of adherent particles in images taken *in situ*.

**Results**

Figure 2 and Table 1 summarize the essential features of the rod and sphere particles in this study. Two batches of silica rods, of aspect ratios 2.5 and 3.2 had average lengths of 1362 and 2639 nm, respectively, rendering the latter substantially more massive. The samples are relatively monodisperse, as gauged by their length and width distributions. The particles are relatively straight-sided as opposed to the rice shapes that are obtained from stretching spheres. The round cap on one end results from rod growth from an emulsion droplet. Worth noting, the fines that were initially present from the synthesis are absent in the final samples. Also important, statistics on particle lengths and widths were obtained from micrographs in which the particles formed a single flat layer (rather than occurring in piles) so that particles could be measured accurately in their flat side-on configurations.

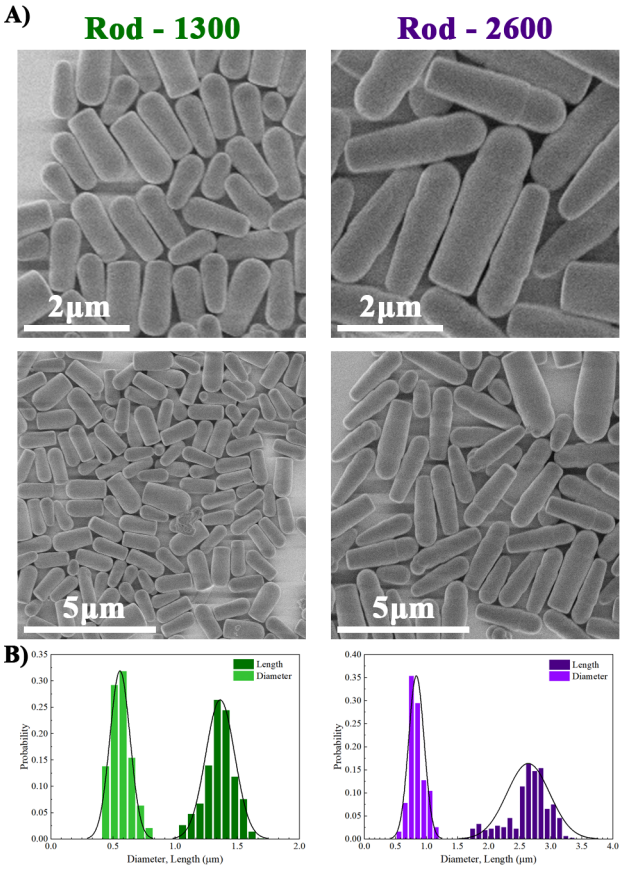


**Figure 2**. (A) Electron micrographs and (B) size and length distributions for Rod-1300 and Rod -2600 samples. The distributions are based on 400-600 particles of each type, far more than those in the images of (A).

**Table I. Properties of Rod and Sphere Samples**

| | Dimensions | | | Diffusivity, $m^2/s$ | |
|---|---|---|---|---|---|
| | Length, nm | Width, nm | Aspect Ratio | Measured | Calculated[16] |
| Rod-1300 | 1362 ±117 | 555 ±80 | 2.48 ±0.25 | --- | $4.59 \times 10^{-13}$ |
| Rod-2600 | 2639 ±345 | 837 ±125 | 3.17 ±0.81 | --- | $2.70 \times 10^{-13}$ |
| | Diameter, nm from measured D | | | Measured | Calculated |
| Sphere-720 | 720 | | | $6.06 \times 10^{-13}$ | --- |
| Sphere-965 | 965 | | | $4.52 \times 10^{-13}$ | --- |
| Sphere-2000 | 2000 (nominal) | | | --- | $2.15 \times 10^{-13}$ |

As check on the lack of fines and the extent to which dimensions measured from electron micrographs are representative of all particles in a sample, we conducted flow cytometry on the Rod-2600 sample. (Particles in the Rod-1300 sample were smaller than the reliable cut off for being counted in the flow cytometer.) For a suspension containing 2340 ppm by weight particles, and for a calculated particle mass of 2.78 $x10^{-12}$g, as described in the Supporting Information for the cylinder dimensions in Table I, we expected there to be 8.27 $x10^{8}$ particles per ml. In fact the flow cytometer counted 8.15 $x10^{8}$ particles per ml upholding this result. This consistency of the weight average and number average concentrations in our samples is a check on sample monodispersity and ensures rigor in the quantitative interpretation of particle capture data, since particle suspensions are weighed, but captured particles are counted visually. For instance, the presence of fines and polydispersity would produce a discrepancy between the two measures of particle concentration that would produce systematic error in interpretation of particle capture studies.

The spherical particle specimens synthesized were also monodisperse and their reported sizes are based on the light scattering data from the Zetasizer. With the larger particles more massive and prone to settling in the Zetasizer, calculated diffusivities were employed from the treatment of Ortega and Garcia de la Torre:[16]

$$D = \frac{1}{3}\frac{kT\,(\ln(AR) + C)}{\pi\,\eta\,L} \qquad (1)$$

kT is the Boltzmann constant times the absolute temperature, AR is the rod's aspect ratio, η is the solvent viscosity, L is the rod length and

$$C = 0.312 + \frac{0.565}{AR} - \frac{0.10}{AR^2} \qquad (2)$$

***Particle Deposition Kinetics***

Following flow of dilute pH 7.4 phosphate buffer through the chamber, suspensions of particles the same buffer were flowed at a gentle shear rate of $22s^{-1}$ through a laminar slit flow chamber and particles were monitored on video as they adhered to the vertical PLL-coated channel wall. This flow chamber orientation avoided gravitational forces normal to the test surface. The dilute buffer maintained pH and, with Debye length of 4.0 nm, electrostatic attractions between flowing a particles and the PLL-coated channel wall were attractive and of relatively long range.

Figure 3 provides examples of progressive particle accumulation on the channel wall, including a panel of images and plots of particle counts as a function of time. For the two rod samples, studies were done at 3 concentrations in the range 125-500 ppm. One example is shown with two runs at a concentration of 125 ppm, to demonstrate the tight reproducibility of the experiments. Additional runs summarized in the Supporting Information were conducted for the spherical particles. In all cases particles are firmly arrested and are not removed by continued exposure to flowing buffer. A key feature in Figure 3 is that the particle accumulation is linear in time on a given surface. This indicates that particles already adhered to the surface do not influence the capture of new particles at the conditions and low coverage levels in this study. The slopes of the particle accumulation plots follow a clear linearity.

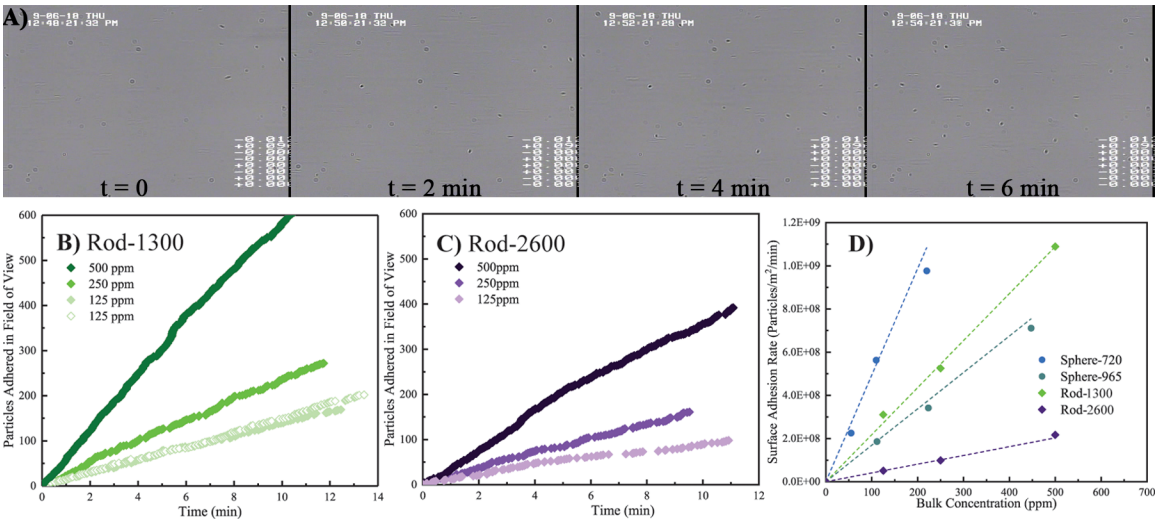


**Figure 3**. Accumulation of flowing particles on PLL coated channel wall. A) Example video micrographs for Rod -2600 from a bulk solution concentration of 250 ppm and a field of view of 260 µm x 177µm B) Example particle capture runs for Rod-1300 sample, from runs with different bulk solution concentrations. Field of view is 260 µm x 177µm. Two runs are included for the concentration of 125 ppm to demonstrate reproducibility. C) Example particle capture runs for Rod-2600 sample, from runs with different bulk solution concentrations. Field of view is 480 µm x 340 µm. D) Summary of particle capture rates as a function of concentration for different particle types. Accumulation rates for suspensions 2 µm sphere are not included in part D because they are off the scale. They are detailed in the supporting information.

With particle capture influenced only by particle-surface interactions and not by particle-particle interactions in solution or on the surface, one expects a proportionality between the rate of particle accumulation ($\frac{d\Gamma}{dt}$), (the slopes of the curves in Figures 3B and 3C) and the bulk solution concentration:

$$\frac{d\Gamma}{dt} = K\, C_{bulk}$$

In general *K,* the rate coefficient*,* could be an intrinsic rate constant, or in the case that particle capture is limited by diffusion from the bulk solution to the interface, *K* would be a *transport coefficient*. In either case, this form motivates the plot in Figure 3D, demonstrating the expected linear proportionality between the particle capture rate and the bulk solution concentration for each particle type. The slopes of the curves in Figure 3D and additional data including that for

spheres in the Supporting Information give *K,* with values summarized in Figure 4. Alternately, *K* can be calculated directly using equation 3 and the accumulation rate in a given particle capture run.

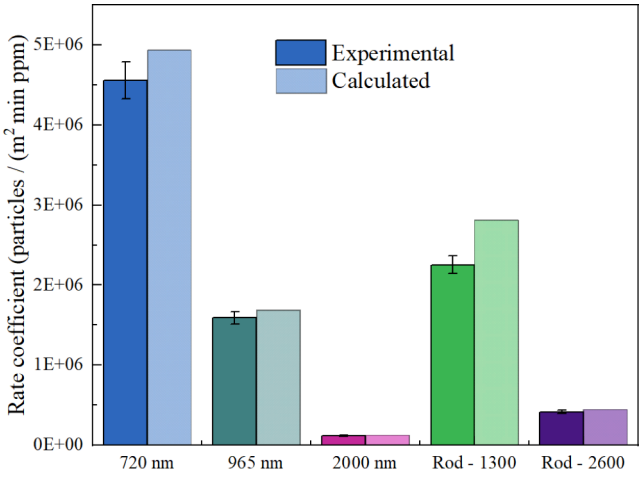


**Figure 4**. Comparison of measured rate constants to those calculated using the Leveque equation (4). Experimental error is estimated to be ~5% based on replicate data sets.

Transport limited capture gives the maximum possible particle accumulation rate. Even in the case where the intrinsic rate constant for particle adhesion is fast, particles can accumulate on the surface only as fast as they arrive from bulk solution. In this transport limited case, when the collecting surface capacity is sufficiently large that particle capture proceeds for a relatively long time, the concentration boundary layer becomes fixed in time during a substantial portion of the run (producing the linear capture curves in Figures 3B and 3C). Here the Leveque solution[38] to the convection-diffusion equation applies and *K* depends on the wall shear rate γ, the distance from the flow chamber entrance to the point of observation, x, and the diffusion coefficient to the adsorbing species, D.

$$K = 0.538\left(\frac{\gamma D^2}{x}\right)^{1/3} \quad (4)$$

Since the wall shear rate and the flow chamber geometry are known, the only variable needing to be addressed is the diffusion coefficient. When using equation 4 to estimate a transport coefficient, we employed the diffusivity values from Table I. The resulting calculated transport coefficients are summarized in Figure 4 alongside the experimentally-measured values.

There is excellent agreement between observed and predicted transport-limited capture rates for rods and spheres alike. This establishes that for dilute solutions of rods, with aspect ratios around 3 and up to ~3 μm in length, strong electrostatically-driven capture, such as that engineered here for cationically-functionalized walls, is rate-limited by particle diffusion to the channel wall. The same is true for spherical particles, even relatively large ones of 2 μm diameter. In fact, Equation 4 has been established for silica spheres up to 1 um in diameter for a range of wall shear rates,[39] but the current finding shows that diffusion-limited capture extends to larger spheres if the surface is sufficiently adhesive. The ability of diffusion-limited kinetics to describe the capture rates of relative large 2-3 μm rods and spheres might be surprising, as the Pectlet number, defined Lu/D (with L a particle dimension such as diameter or length, and u, the streamline velocity of a near-wall particle) falls in the range 1-10. The observations indicate that while viscous forces may be important in particle transport, it is ultimately diffusion perpendicular to the wall in the boundary layer that controls particle capture.

Also of interest, the diffusivities from Table I for the rods apply for quiescent conditions. The use of quiescent diffusivities in equation 4 to accurately predict particle capture demonstrates

that the velocity gradient is not so strong as to orient particles and to produce a biased diffusivity in the experiments.

***Mass Accumulation: Spheres versus Rods***

Studies with ellipsoidal rods made from stretched sphere have compared the accumulated mass from rod and spherical particles of identical volume (also identical mass).[27] These studies have led, for some samples, to the conclusion that, even in the limiting case of dilute solutions and in a slit-shear channel such as ours (with wall shear rates in the range 15-22 $s^{-1}$), rods more effectively deliver particles than spheres. While the spherical and rod particles in the current study are not paired in terms of equivalent particle volumes, the tight adherence of the observed capture rates to transport-limited capture allows a comparison of spheres and rods of equal volume in this limit. Indeed taking the ratio of the transport coefficient for rods to that for spheres in the same flow experiment reveals that only differences in the diffusion coefficient will lead to differences in the accumulation rate. Furthermore, using equations 1 and 2 for the rod diffusivity, and normalizing by the Stokes Einstein form for a sphere of equal volume, the ratio of transport coefficients depends only on the rod aspect ratio:

$$\frac{K_{rod}}{K_{sph}} = \left(\frac{D_{rod}}{D_{sph}}\right)^{2/3} = \left(\frac{(C+\ln(AR))}{\left(\frac{2\,AR^2}{3}\right)^{1/3}}\right)^{2/3} \tag{5}$$

where C is defined in equation 2.

The plot of equation 5 in Figure 5 reveals that the ratio of transport coefficients, (equal to the rate of mass delivery by rods normalized by that on spheres), is slightly less than unity for rods of modest aspect ratio such as our. Further, the ratio decreases only slightly as the aspect ratio increases, up to 10, well beyond the range of practicality for delivery applications.

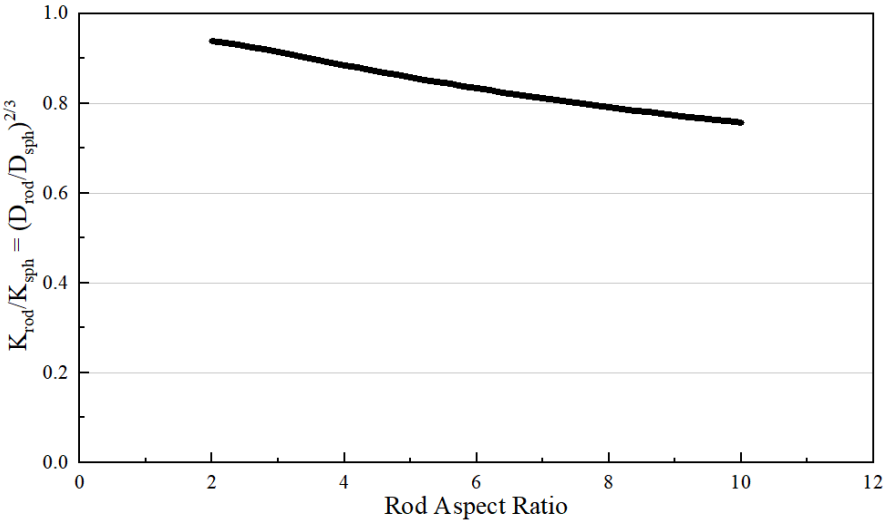


**Figure 5.** Transport rate coefficient for rod shaped particles normalized by that for spheres, calculated via equation 4, for adhesion to a channel wall in laminar flow.

Thus for transport limited particle capture (where the binding events that trap the particle are rapid and where hydrodynamic forces and particle rotation does not interfere with capture), and where a shear gradient does not alter the rod diffusivity, spheres are slightly *more efficient* than rods of the same volume in delivering material a channel wall. Reports to the contrary in other labs are likely a result of weaker or slower binding kinetics than expected.

***Rod orientation on the collecting surface.***

For the larger rod particles, Rod-2600, it was possible to examine the orientations of the adhered rods using a 40x objective after monitoring deposition at 10x or 20x. After particles were

deposited from a buffered suspension of flowing rods at a wall shear rate of $22s^{-1}$, flowing buffer was reintroduced. During this process, the surface was observed at 10x or 20x to ensure that no captured particles were removed. The objective was then switched to 40x and images recorded at the original point of observation along with other positions on the slide, at roughly the same distance from the channel entrance. After sufficient numbers of images were captured, the pump was turned off and the system was allowed to equilibrate for 10 minutes before additional images were captured.

Sufficient micrographs to produce data for 600 particles, each with and without flow, revealed a variety of orientations both normal to the surface and in the plane of the surface. Regarding rod orientation normal to the surface, as indicated in the schematic and example video-micrograph frame of Figure 6, the rods were sometimes adsorbed standing on end, but also sometimes appeared to be substantially tipped, though it was difficult to say when particle were truly lying

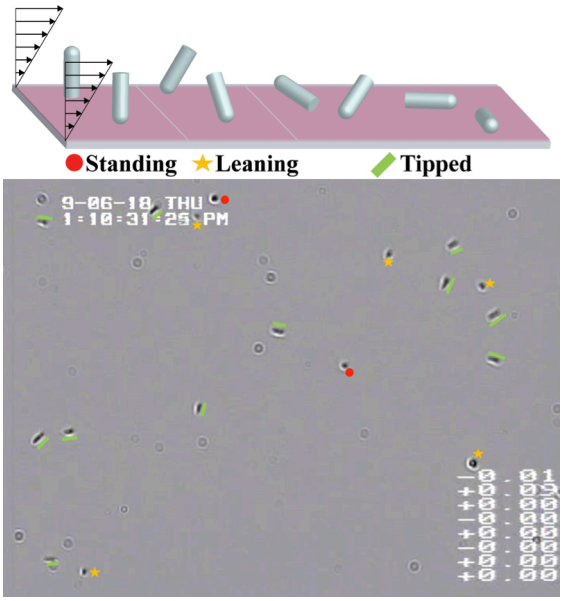


**Figure 6**. Schematic showing rod orientations normal to the surface, and an example micrograph showing, in color, how rod orientations were assigned. Image recorded without flow.

on their sides. There were also intermediate orientations where the rods were anchored at one end and leaning somewhat. The leaning rods appear shorter than average lengths observed in the electron micrographs. By contrast the rods designated as tipped revealed their elongated shapes, as a result of their orientations. The proportions of standing (near vertical), leaning, and tipped orientations are indicated in the pie charts of Figure 7, for images taken during and after flow. The pie charts reveal no significant impact of gentle flow on these three categories of surface-normal orientation and also that there is a substantial fraction of particles trapped in vertical or tipped orientations (insensitive to gentle shear). This might be considered surprising since a completely flat side-on (fully tipped) orientation should be preferred because of its greater adhesive contact area. The fact that standing and leaning orientations persist suggests that binding is quite strong relative to hydrodynamic force. The existence of near vertical trapped configurations suggests that, when rods adhere by their ends, they can become trapped before rotating flat to the surface.

Figure 7 summarizes the in-plane rod orientation of captured side-on rods (300-350 particles each with and without flow). An angle of zero corresponds to rods oriented in the flow direction while 90° is perpendicular to the flow but relatively flat to the surface. The distribution in the histogram would be uniform over the full range of angles for random particle orientation; however, there is a modest preference for orientation of captured rods in the flow direction. There is no statistically significant impact of stopping the flow after rods have adhered, suggesting that the bound rods are immobile. The slight orientation of captured rods might be a result of slight orientation of free rods during flow near the surface and prior to capture (with hydrodynamics competing with diffusive rotation), or it could result from the capture process itself. For instance a rod oriented away from zero degrees upon its first contact, possibly by an

end, could experience a torque that orients the rod in the flow direction before it becomes completely immobilized. The lack of substantial orientation suggests that adhesion was established before most rods had time to fully orient.

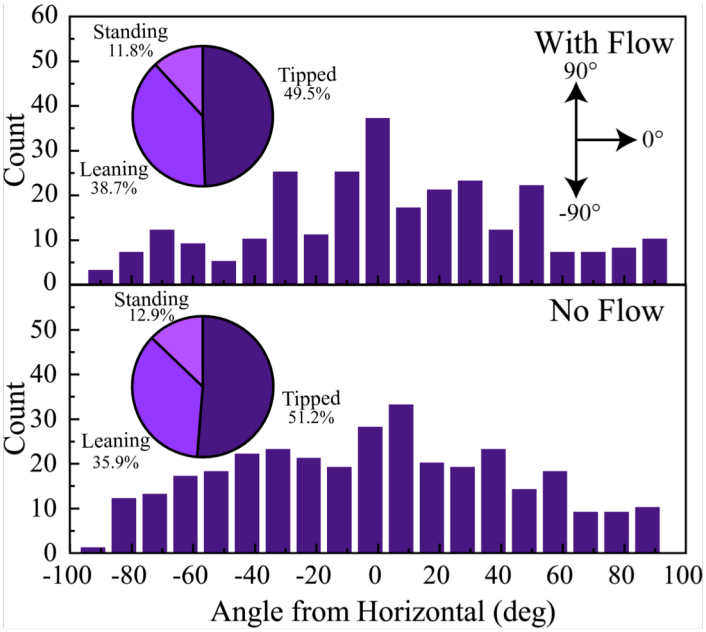


**Figure 7.** Summary of rod orientation with and without flow, as indicated. Orientation normal to the surface is summarized in pie charts. Angular rod orientation is indicated in the bar graphs.

## Conclusions and Significance

This study addressed the capture of rod-shaped silica microparticles from gentle shear flow onto the walls of flow channels where attractive electrostatic (and van der Waals) surface forces dominated the particle-wall interactions, producing a long-range driving force for rapid particle capture. Experiments were configured so that gravity did not cause sedimentation towards or away from the surface. The aspect ratios of two silica rod samples were in the neighborhood of 2.5-3.2 and two particles sizes were studied. Notably the larger particles approached the size and

shape of *E. coli* bacteria (albeit lacking flagella or pili). The study focused on the dilute particle regime both in suspension and on the surface.

The capture rates of rod particles on the flow channel wall were proportional to the bulk solution particle concentrations, with rate coefficients in excellent quantitative agreement with the calculated transport coefficients. The calculation included a diffusion coefficient for each particle type in dilute quiescent conditions. The observed particle capture rates for spheres also agreed with their respective calculated transport-limited rates, a control that provided perspective on the rod capture. The observed transport limited particle capture reaffirmed that long range electrostatic attractions not only produce strong particle binding but that the capture events themselves are rapid compared with transport time scales, including that for particle rotations. That this should be true for rod-shaped particles is not obvious, since rod rotation limits close contact with the channel wall.[23] The transport-limited rod capture, with its implication that the rod-capture events are rapid, also suggests that rod rotations in the near-surface shear field are sufficiently fast so that particle ends encounter the surface rapidly relative to the arrival of rods from solution. Alternately it suggests that even these relatively large rod particles experience sufficient diffusion to enhance particle-wall contact over what it would be without diffusion.

We demonstrated that in the transport limit and when the rod diffusivity is not appreciably altered by orientation from shear, the mass or numbers of rods captured on a surface is actually slightly less than spheres of equivalent volume and becomes increasingly smaller relative to equivalent spheres as the rod aspect ratio is increased. This fact contradicts some experimental

studies in other labs. The discrepancy may be a result of the fundamentally slower (surface binding limited) capture rates in those studies, for instance involving antibody binding.

The substantial mix of different captured rod configurations, standing versus leaning or tipped, also attests to the rapid nature of binding events upon initial particle-wall contact: Sufficiently strong binding is established on timescales shorter than particle rotation, so that when a rod end encounters the wall, the rod arrests in an end-on or slightly tipped configuration. Binding is sufficiently tight to prevent the rod from rotating to establish a greater contact area with wall in a side-contact configuration. Even so, there is evidence that, for some fraction of particles, when rods encounter the wall, they align slightly with the flow before final arrest. (We cannot prove that this modest alignment does not occur during flow and prior to encounters with the wall; however, any flowing rod orientation is sufficiently weak that an isotropic translational diffusion coefficient is found to govern transport from bulk solution to the interface.)

The current work suggests that transport limited capture of rods results from the rapid adhesion events that dominate the initial particle contact and trap particles in configurations (such as protruding end-on) where they experience a maximum shear (as opposed to lying flat). At this transport limit, spherical delivery vehicles out-perform rods of equivalent volume. In filtration applications, rods may be slightly more difficult than spheres to be captured on membranes with large straight pores, however, once some rods are captured, substantial populations may protrude from the pore wall to reduce the flux. Finally with regard to bacterial capture, the potential to control the orientation and configuration of deposited cells is fascinating, as others have

suggested that cell orientation influences biofilm growth and the amount of biomass needed to establish a colony.[40]

***Acknowledgements***
This work was supported by and NSF 1848065 and a Chemistry-Biology Interface Training Fellowship to MKS, through National Research Service Award T32 GM008515 from the National Institutes of Health. MMS and ZX wish to thank Mark Tuominen for helpful discussions and Amy Burnside for flow cytometry experiments.

**References**


1. Yang, J. L.; Bos, R.; Poortinga, A.; Wit, P. J.; Belder, G. F.; Busscher, H. J. Comparison of particle deposition in a parallel plate and a stagnation point flow chamber. *Langmuir* **1999**, *15*, 4671-4677.

2. Meinders, J. M.; Busscher, H. J. Adsorption and Desorption of Colloidal Particles on Glass in a Parallel-Plate Flow Chember- Influence of Ionic-Strength and Shear Rate *Colloid Polym. Sci.* **1994**, *272*, 478-486.

3. Patil, V. R. S.; Campbell, C. J.; Yun, Y. H.; Slack, S. M.; Goetz, D. J. Particle diameter influences adhesion under flow. *Biophys. J.* **2001**, *80*, 1733-1743.

4. Duffadar, R.; Kalasin, S.; Davis, J. M.; Santore, M. M. The impact of nanoscale chemical features on micron-scale adhesion: Crossover from heterogeneity-dominated to mean-field behavior. *J. Colloid Interface Sci.* **2009**, *337*, 396-407.

5. Kalasin, S.; Santore, M. M. Non-specific adhesion on biomaterial surfaces driven by small amounts of protein adsorption. *Colloid Surf. B-Biointerfaces* **2009**, *73*, 229-236.

6. Decuzzi, P.; Gentile, F.; Granaldi, A.; Curcio, A.; Causa, F.; Indolfi, C.; Netti, P.; Ferrari, M. Flow chamber analysis of size effects in the adhesion of spherical particles. *Int. J. Nanomed.* **2007**, *2*, 689-696.

7. Lee, S. Y.; Ferrari, M.; Decuzzi, P. Shaping nano-/micro-particles for enhanced vascular interaction in laminar flows. *Nanotechnology* **2009**, *20*.

8. Gentile, F.; Chiappini, C.; Fine, D.; Bhavane, R. C.; Peluccio, M. S.; Cheng, M. M. C.; Liu, X.; Ferrari, M.; Decuzzi, P. The effect of shape on the margination dynamics of non-neutrally buoyant particles in two-dimensional shear flows. *J. Biomech.* **2008**, *41*, 2312-2318.

9. Li, K.; Ma, H. L. Deposition Dynamics of Rod-Shaped Colloids during Transport in Porous Media under Favorable Conditions. *Langmuir* **2018**, *34*, 2967-2980.

10. Li, K.; Ma, H. L. Rotation and Retention Dynamics of Rod-Shaped Colloids with Surface Charge Heterogeneity in Sphere-in-Cell Porous Media Model. *Langmuir* **2019**, *35*, 5471-5483.

11. Jeffery, G. B. The motion of ellipsoidal particles in a viscous fluid. *Proc. R. soc. Lond. Ser. A-Contain. Pap. Math. Phys. Character* **1922**, *102*, 161-179.

12. Kim, D. K.; Hyun, J. Y.; Kim, S. C.; Kim, H. S.; Lee, S. Y. Inertial effects on cylindrical particle migration in linear shear flow near a wall. *Microfluid. Nanofluid.* **2016**, *20*.

13. Rosen, T.; Lundell, F.; Aidun, C. K. Effect of fluid inertia on the dynamics and scaling of neutrally buoyant particles in shear flow. *J. Fluid Mech.* **2014**, *738*, 563-590.

14. Tirado, M. M.; Garciadelatorre, J. Translational Friction Coefficients of Rigid, Symmetric Top Macromolecules - Application to Circular Cylinders. *J. Chem. Phys.* **1979**, *71*, 2581-2587.

15. Tirado, M. M.; Garciadelatorre, J. Rotational-Dynamics of Rigid, Symmetric Top Macromolecules - Application to Circular Cylinders. *J. Chem. Phys.* **1980**, *73*, 1986-1993.

16. Ortega, A.; de la Torre, J. G. Hydrodynamic properties of rodlike and disklike particles in dilute solution. *J. Chem. Phys.* **2003**, *119*, 9914-9919.

17. Mukhija, D.; Solomon, M. J. Translational and rotational dynamics of colloidal rods by direct visualization with confocal microscopy. *J. Colloid Interface Sci.* **2007**, *314*, 98-106.

18. Okagawa, A.; Cox, R. G.; Mason, S. G. Kinetics of Flowing Dispersions 6. Transient Orientation and Rheological Phenomena of Rods and Disks in Shear Flow *J. Colloid Interface Sci.* **1973**, *45*, 303-329.

19. Chen, S. B.; Jiang, L. Orientation distribution in a dilute suspension of fibers subject to simple shear flow. *Phys. Fluids* **1999**, *11*, 2878-2890.

20. Gunes, D. Z.; Scirocco, R.; Mewis, J.; Vermant, J. Flow-induced orientation of non-spherical particles: Effect of aspect ratio and medium rheology. *J. Non-Newton. Fluid Mech.* **2008**, *155*, 39-50.

21. Skjetne, P.; Ross, R. F.; Klingenberg, D. J. Simulation of single fiber dynamics. *J. Chem. Phys.* **1997**, *107*, 2108-2121.

22. Stover, C. A.; Cohen, C. The Motion of Rodlike Particles in the Pressure-Driven Flow between 2 Flat Plates. *Rheol. Acta* **1990**, *29*, 192-203.

23. Kaya, T.; Koser, H. Characterization of Hydrodynamic Surface Interactions of Escherichia coli Cell Bodies in Shear Flow. *Phys. Rev. Lett.* **2009**, *103*.

24. Shave, M. K.; Kalasin, S.; Ying, E.; Santore, M. M. Nanoscale Functionalized Particles with Rotation-Controlled Capture in Shear Flow. *ACS Appl. Mater. Interfaces* **2018**, *10*, 29058-29068.

25. Eniola, A. O.; Hammer, D. A. In vitro characterization of leukocyte mimetic for targeting therapeutics to the endothelium using two receptors. *Biomaterials* **2005**, *26*, 7136-7144.

26. Doshi, N.; Prabhakarpandian, B.; Rea-Ramsey, A.; Pant, K.; Sundaram, S.; Mitragotri, S. Flow and adhesion of drug carriers in blood vessels depend on their shape: A

study using model synthetic microvascular networks. *J. Control. Release* **2010**, *146*, 196-200.

27. Seymour, M. B.; Chen, G. X.; Su, C. M.; Li, Y. S. Transport and Retention of Colloids in Porous Media: Does Shape Really Matter? *Environ. Sci. Technol.* **2013**, *47*, 8391-8398.

28. Adriani, G.; de Tullio, M. D.; Ferrari, M.; Hussain, F.; Pascazio, G.; Liu, X. W.; Decuzzi, P. The preferential targeting of the diseased microvasculature by disk-like particles. *Biomaterials* **2012**, *33*, 5504-5513.

29. Decuzzi, P.; Ferrari, M. The adhesive strength of non-spherical particles mediated by specific interactions. *Biomaterials* **2006**, *27*, 5307-5314.

30. Shah, S.; Liu, Y. L.; Hu, W.; Gao, J. M. Modeling Particle Shape-Dependent Dynamics in Nanomedicine. *J. Nanosci. Nanotechnol.* **2011**, *11*, 919-928.

31. Kolewe, K. W.; Kalasin, S.; Shave, M.; Schiffman, J. D.; Santore, M. M. Mechanical Properties and Concentrations of Poly(ethylene glycol) in Hydrogels and Brushes Direct the Surface Transport of Staphylococcus aureus. *ACS Appl. Mater. Interfaces* **2019**, *11*, 320-330.

32. Casa, L. D. C.; Deaton, D. H.; Ku, D. N. Role of high shear rate in thrombosis. *J. Vasc. Surg.* **2015**, *61*, 1068-1080.

33. Li, W. B.; Ji, W. J.; Sun, H. H.; Lan, D.; Wang, Y. R. Pattern Formation in Drying Sessile and Pendant Droplet: Interactions of Gravity Settling, Interface Shrinkage, and Capillary Flow. *Langmuir* **2019**, *35*, 113-119.

34. Kuijk, A.; Imhof, A.; Verkuijlen, M. H. W.; Besseling, T. H.; van Eck, E. R. H.; van Blaaderen, A. Colloidal Silica Rods: Material Properties and Fluorescent Labeling. *Part. Part. Syst. Charact.* **2014**, *31*, 706-713.

35. Kuijk, A.; van Blaaderen, A.; Imhof, A. Synthesis of Monodisperse, Rodlike Silica Colloids with Tunable Aspect Ratio. *J. Am. Chem. Soc.* **2011**, *133*, 2346-2349.

36. Li, W. L.; Lu, K.; Walz, J. Y.; Anderson, M. Effects of Rod-like Particles on the Microstructure and Strength of Porous Silica Nanoparticle Composites. *J. Am. Ceram. Soc.* **2013**, *96*, 398-406.

37. Stober, W.; Fink, A.; Bohn, E. Controlled Growth of Monodisperse Silica Spheres in Micron Size Range *J. Colloid Interface Sci.* **1968**, *26*, 62-&.

38. Leveque, M. A. Les Lois de la Transmission de Chaleur par Convection. *Ann. Mines* **1928**, *13*, 201-299.

39. Kalasin, S.; Santore, M. M. Hydrodynamic crossover in dynamic microparticle adhesion on surfaces of controlled nanoscale heterogeneity. *Langmuir* **2008**, *24*, 4435-4438.

40. Duvernoy, M. C.; Mora, T.; Ardre, M.; Croquette, V.; Bensimon, D.; Quilliet, C.; Ghigo, J. M.; Balland, M.; Beloin, C.; Lecuyer, S.; Desprat, N. Asymmetric adhesion of rod-shaped bacteria controls microcolony morphogenesis. *Nat. Commun.* **2018**, *9*.